Document Change Log

Revision	Date	Affected Portions and Description
	4 April 2018	Original release

Which Product Versions Does this Document Cover?

Product Filename Prefix	Version Number in Filename	Brief Description
AirMSPI_ER2_GRP_ELLIPSOID	V006	L1B2 Ellipsoid-Projected Georectified Radiance and Polarization Data
AirMSPI_ER2_GRP_TERRAIN	V006	L1B2 Terrain-Projected Georectified Radiance and Polarization Data

TABLE OF CONTENTS

1 INTRODUCTION

The purpose of this document is to describe the data quality of the AirMSPI L1B2 products specifically for the Aerosol Characterization from Polarimeter and Lidar (ACEPOL) field campaign, which was based out of NASA Armstrong Flight Research Center (AFRC) in Palmdale, CA and included flights over California, the Pacific Ocean, and Arizona. AirMSPI imagery was acquired from 19 October to 9 November 2017.

1.1 AirMSPI L1B2 Products

The Airborne Multiangle SpectroPolarimetric Imager (AirMSPI) Level 1B2 products contain radiometric and polarimetric observations of clouds, aerosols, and the surface of the Earth made from the National Aeronautics and Space Administration's (NASA's) ER-2 high-altitude research aircraft. The AirMSPI instrument acquires data using one of two possible modes, step-and-stare and sweep. Step-and-stare data are gridded with 10 m spatial sampling, with one file provided for each view angle. Sweep data are gridded with 25 m spatial sampling. Files are distributed in HDF-EOS-5 format.

The instrument reports for eight spectral bands (355, 380, 445, 470, 555, 660, 865, and 935 nm) the incident radiance (Stokes *I)*, complemented with the linear polarization state (Stokes *Q* and *U*) in three of the bands (470, 660, and 865 nm) for a total of 14 channels.

1.2 AirMSPI Data Processing and Distribution

The MISR Science Computing Facility (SCF) at the Jet Propulsion Laboratory (JPL) supports the development of AirMSPI science algorithms and software, instrument calibration and performance assessment, and also provides quality assessment and data validation services with respect to AirMSPI Science Data Processing (SDP). The MISR SCF is used to perform the standard processing of the AirMSPI data. After AirMSPI data processing is complete, the standard output products are archived and made available to users via the Langley Research Center (LaRC) Atmospheric Science Data Center (ASDC) client services. See https://eosweb.larc.nasa.gov/project/airmspi/airmspi_table.

1.3 Controlling Documents

1) Multiangle Spectropolarimetric Imager (MSPI) Algorithm Theoretical Basis Document Rev. B Draft, November 2009 (or latest version).

1.4 Related Documents

1) AirMSPI Data Product Specification for the AirMSPI Level 1B2 Products (V006), JPL D-100825, Rev. C, September 2017 (or latest version).

2 RADIOMETRIC CALIBRATION

2.1 Laboratory Calibration

Laboratory radiometric calibration of the AirMSPI instrument (Diner et al., 2013a) was conducted on 8 September 2017 (prior to the ACEPOL field campaign) by observing the output port of a 1.65 m integrating sphere. The sphere illuminates the entire field of view of the instrument. Data were collected at multiple light levels and the sphere output was monitored with an Analytical Spectral Devices (ASD) FieldSpec Pro spectrometer in order to generate a digital number (DN) vs. radiance regression for each pixel. The AirMSPI line arrays have 1536 pixels in each channel. Offset levels are determined from observations in 100 pixels at the end of each array that are shielded from illumination; hence only 1436 pixels in each line collect image data. After correction for non-linearity (lincal), gain factors are computed on a per-pixel basis for each channel. The 13 spectral channels of the instrument measure incident radiance at wavelengths close to 355, 380, 445, 470, 555, 660, 865, and 935 nm (8 bands). In keeping with Stokes parameter nomenclature, the polarization channels report I, Q, and U, where I is the total measured radiance. The Stokes parameters Q (excess of horizontally over vertically polarized light) and U (excess of 45° over 135° polarized light) are reported for the bands at 470, 660, and 865 nm. Note that the AirMSPI instrument does not have a separate radiance-only channel at 470 nm. The radiance reported in the AirMSPI data products for this channel is obtained independently from the demodulated 470Q and 470U channel data and is the mean of the values derived from these two channels. Thus, although the AirMSPI instrument itself only has 13 spectral channels, 14 spectral channels are reported in the AirMSPI L1B2 products.

Although gain factors are derived on a per-pixel basis, residual striping can appear in Earth images, particularly in the UV bands. It is believed that this striping is the result of out-of-band spectral leakage due to physical imperfections in the focal plane filter.

2.2 Vicarious Calibration

On 25 October 2017, as part of the ACEPOL campaign, AirMSPI overflew the Rosamond Lake dry lake bed to the north of Lancaster, CA. Data were taken both from the air, and by a field team on the ground. For the latter, measurements were made of the reflectance of the lake bed, the surface pressure, and the aerosol loading. Instrumentation included an ASD field spectrometer, two Microtops II sunphotometers, and the GroundMSPI instrument (Diner et al., 2012). Relevant information was used as input to a Markov chain radiative transfer code, which calculates top-of-atmosphere spectral radiances. The Markov chain code is a vector code, tracing polarization components through the atmosphere (Xu et al., 2010). This vicarious calibration of AirMSPI had band-dependent agreement with the laboratory calibration. Differences ranged from 15% in the UV to 2% in the mid-visible. The radiometric calibration of AirMSPI for the entire ACEPOL campaign was set using this vicarious calibration. It is believed to have a higher accuracy than the laboratory calibration, due to the low UV light levels used to calibrate AirMSPI in the laboratory.

2.3 Calibration Traceability

AirMSPI calibrations are traceable to *Système international* (SI) Units, via National Institute of Standards and Technology (NIST) standards. For laboratory calibrations, this is accomplished through a reference 20.32 cm (8 inch) integrating sphere, calibrated annually by the vendor, Gooch & Housego (http://goochandhousego.com/). For vicarious calibrations, this is done through a Spectralon reflectance standard located at the vicarious calibration site.

2.4 Radiometric Data Quality Indicators

Following the practice adopted by the Multi-angle Imaging SpectroRadiometer (MISR) project, each AirMSPI pixel is assigned a Radiometric Data Quality Indicator (RDQI). The RDQI definitions are as follows:

RDQI = 0: No radiometric issues are identified.

RDQI = 1: The radiometric quality does not meet an identified threshold but is deemed usable for scientific analysis purposes.

RDQI = 2: The radiometric quality does not meet a secondary threshold and the data from this pixel should not be used for scientific analysis purposes.

RDQI = 3: The quality of the pixel is scientifically and cosmetically unusable. In addition, the shielded pixels at the end of each line array are marked with an RDQI of 3.

During laboratory calibration, a "gain" is computed from the slope of camera output DN to total-band incident radiance, I. It is observed that pixels with a large out-of-band leakage have a larger uncertainty in this gain, in that it is observed to vary with the spectrum of the incident light. A data quality indicator can thus be computed based on the change in gain with different illumination sources. Specifically, we take the ratio of the gain computed with an incandescent lamp to the gain computed from adding a UV plasma lamp. Pixels for which this gain ratio is between 0.95 and 1.05 are assigned an RDQI value of 0 indicating that out-of-band light is a small contributor to the measured radiance. Pixels for which the gain ratio is outside of this range, but between 0.90 and 1.10 are assigned an RDQI value of 1. Pixels with gain ratios outside both these ranges, but between 0.80 and 1.20 are assigned an RDQI value of 2. All other pixels are assigned an RDQI value of 3. Note that for the 470I channel, for which the reported radiance is the mean of the demodulated 470Q and 470U channel data, the RDQI is likewise calculated as the mean (rounded to the nearest integer) of the RDQI values for these two channels. The observed out-of-band leakage is believed to be the cause of permanent striping in the images, which is particularly noticeable in the UV bands.

Pixels marked with RDQI = 0 are expected to have an absolute radiometric uncertainty of ~5% (1σ). This radiometric uncertainty is attributed to the vicarious calibration methodology, which sets the absolute radiometric scale. The laboratory calibration is used to establish the relative-pixel response, also known as "flat-fielding."

3 SPECTRAL CALIBRATION

Determination of the detailed spectral response function (SRF) of each AirMSPI channel has been made based on the laboratory calibration of 9 December 2013. A monochromator was used for this purpose. The SRF is equal to the camera response to monochromatic light normalized by a silicon diode response. The monochromator provided wavelength scans from 300 to 2500 nm. Two sources were used in separate spectral scans of all channels — a Luxim Light Emitting Plasma lamp for ultraviolet-blue, and a quartz-halogen lamp for the remaining visible and near-infrared channels. The results of this calibration are shown in Table 1 and Figure 2.

In the current product release (V006), center wavelengths, effective (equivalent square-band) bandwidths, and effective (equivalent square-band) transmittances are calculated by applying the moments method of Palmer (1984) to the normalized spectral response of each band over the range 300-1100 nm. Solar irradiances are weighted by the total-band spectral response. The Wehrli (1985) extraterrestrial solar spectrum was used for this purpose. These values are provided in Table 1 below, and represent the total-band response.

In general, radiometric response at wavelengths far from the "in-band" spectral region is estimated at $< 10^{-4}$ of the peak response, though as noted above, a larger amount of out-of-band leakage is present in a small subset of pixels in the UV bands, leading to striping in a portion of the UV images. Currently uncorrected striping in the 355 and 380 nm bands is attributed to filter blemishes that create a scene-dependent scattered light response.

Table 1 – Total-band effective center wavelength, bandwidth and transmittance, and total-band weighted solar irradiance E_0 [W m^{-2} nm^{-1}] at 1 AU

Channel Name	Center Wavelength (nm)	Effective Bandwidth (nm)	Effective Transmittance	Solar Irradiance (W m^{-2} nm^{-1})
355I	355.1	47.7	0.609	1.002
380I	377.2	40.4	0.750	1.079
445I	443.3	46.0	0.799	1.861
470I	469.1	45.5	0.824	2.000
470Q	469.4	45.0	0.837	1.999
470U	468.8	46.0	0.815	2.000
555I	553.5	38.6	0.758	1.857
660I	659.2	45.2	0.835	1.555
660Q	659.1	43.8	0.881	1.556
660U	659.1	48.2	0.798	1.556
865I	863.3	43.5	0.829	0.976
865Q	863.7	45.6	0.810	0.976
865U	864.1	48.5	0.753	0.975
935I	931.3	53.2	0.809	0.823

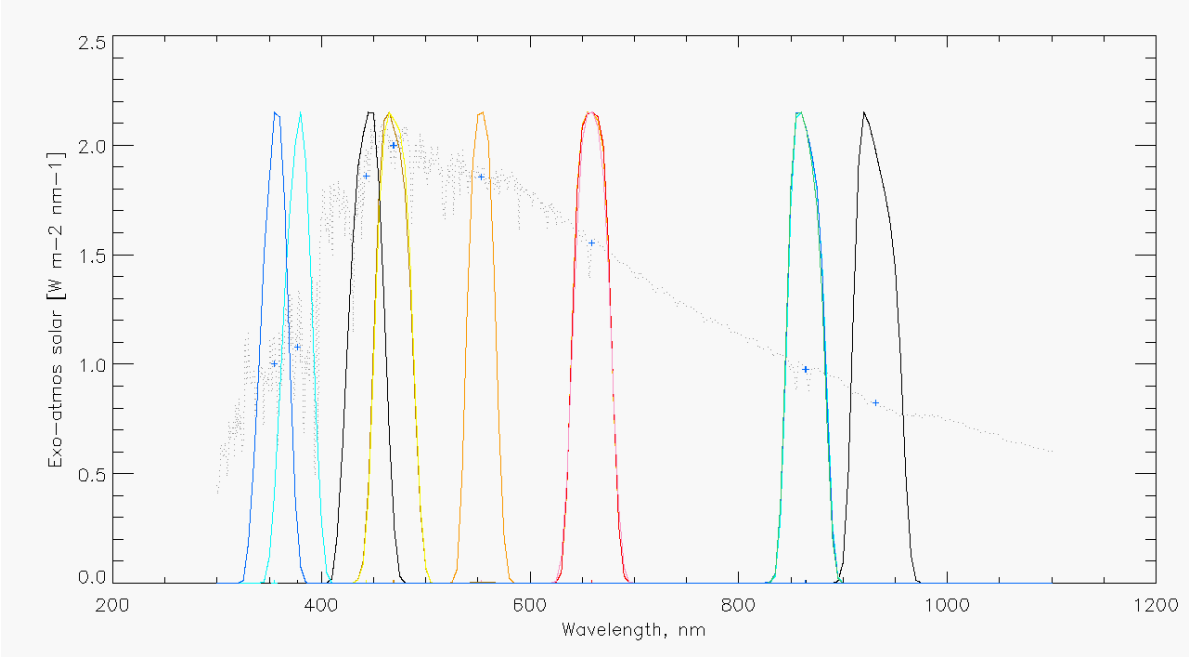

Figure 2. AirMSPI spectral response functions (SRF) shown in colored lines with the Wehrli (1985) exoatmospheric solar irradiance values shown in the faint, gray, dotted line. E0 values at 1 AU are indicated by the "+" symbol.

4 POLARIMETRIC CALIBRATION

AirMSPI uses a time-varying retardance in the optical path to modulate the orientation of the linearly polarized component of the incoming light, described by the Stokes components Q (excess of horizontally over vertically polarized light) and U (excess of 45º over 135º polarized light) (Diner et al., 2007, 2010; Mahler et al., 2011). As a result, the ratios of these parameters to the radiance I, given by $q = Q/I$ and $u = U/I$ are to first order insensitive to the absolute radiometric calibration of a given pixel because both the numerator and denominator are determined from signals acquired by the same detector element. The degree of linear polarization (DoLP) and angle of linear polarization (AoLP) derived from these ratios, equal to $\sqrt{q^2 + u^2}$ and $0.5\tan^{-1}(u/q)$, respectively, are likewise insensitive to absolute radiometric calibration, based on similar considerations. To compensate for instrumental polarization aberrations (e.g., mirror diattenuation, imperfect retardance), a set of 10 polarimetric calibration coefficients is established for every pixel (Diner et al., 2010).

Two specialized pieces of equipment exist for verifying and controlling the performance of the polarimetric measurement approach during in-flight operations of AirMSPI. The first is an optical probe, which continuously sends a beam of light through the photoelastic modulators (PEMs) to monitor their retardances and phases. The information from the probe shows how far the PEM retardances and phases are from their desired values. A feedback control system within the instrument then adjusts the PEM parameters to drive the error signals to zero. Test data demonstrated the ability to control the PEM retardance and phase parameters to within a fraction of 1 mrad, keeping contributions to the overall DoLP uncertainty budget at <0.001. The second polarization monitoring system is an external polarization validator, which consists of nine light-

emitting diodes (LEDs), three each at the AirMSPI polarimetric bands, that illuminate a plastic diffuser. In front of the diffuser, sheet polarizers are placed in different orientations. The validator is viewed before and after every multiangle observation of an Earth scene. Information from the validator system is used to derive instrument dark current and evaluate the stability of the DoLP measurements.

Results from a ground-based version of the instrument, GroundMSPI (Diner et al., 2012), show systematic DoLP uncertainties (excluding the effects of random noise), determined as the root-mean-square residual in DoLP as a polarizer is rotated in front of the camera, of ±0.003 or better. Results for AirMSPI, using the rotating polarizer methodology described in Diner et al. (2010), show similar residuals.

5 GEORECTIFICATION AND CO-REGISTRATION

As a part of the ground data processing, AirMSPI data from all spectral bands and all viewing angles are georectified and co-registered to a common Earth-based, Universal Transverse Mercator (UTM) projection grid. Distortions that can be associated with AirMSPI's type of pushbroom remote sensing imaging are taken into account by properly defining instantaneous pixel projection rays using ancillary data such as estimates of camera internal viewing geometry and ER-2 navigation data, which provide dynamic measures of the platform altitude and attitude variations. There are two types of AirMSPI georectified data products: 1) terrain projected and 2) ellipsoid projected. Terrain-projected data use a digital elevation model (DEM) for the projection surface so that cloud-free imagery is truly orthorectified with reference to that surface. Ellipsoid-projected data use the World Geodetic System 1984 (WGS84) Earth reference ellipsoid for the projection surface. One purpose of the ellipsoid projection is to provide input to stereoscopic height retrievals for predominantly cloudy imagery. Automatic stereoscopic retrieval software is currently in development.

Factors affecting geospatial accuracy of AirMSPI products include: 1) relative band-to-band co-registration within a single viewing angle, 2) multi-angle co-registration, and 3) absolute georectification. The uncertainty depends on the magnitude of the errors in the supplied ancillary data and errors in the projection surface defined by the DEM. In the case of the ACEPOL campaign, data acquired entirely over the ocean surface are processed into ellipsoid-projected data products only. For data sets acquired over land a terrain-projected data product is also derived based on the United States Geological Survey (USGS)-provided National Elevation Dataset (NED) with 10 m horizontal posting and 2.44 m rms error in elevation. Errors in the ancillary data defining viewing geometry are handled as static and dynamic pointing errors in order to characterize them using available ground control points (GCPs) in a procedure based on simultaneous bundle adjustment (Jovanovic et al., 2012). For targets where there is an optimum number of GCPs available, both static and dynamic pointing errors are recovered simultaneously prior to georectification and co-registration. These data are denoted as having full geometric calibration "directly" applied with expected co-registration and georectification uncertainty of around 15 m rms across all viewing angles and all bands. For other targets, (i.e., those without available GCPs, which are mostly fully ocean or cloudy imagery), an estimate of static pointing errors made on separate flight lines within the same campaign is utilized. These products are denoted as having geometric calibration "indirectly" applied with a current estimate of

georectification and co-registration uncertainty of less than one hundred meters. The type of geometric calibration is recorded in the file metadata list under the field name "Geolocation stage". Analysis and implementation efforts are still in progress with an objective to fully optimize the camera viewing model so that uncertainties of indirectly calibrated data are minimized.

Band-to-band relative co-registration uncertainty within the same viewing angle is well within 10 m, which is the pixel size of the map projection grid in the step-and-stare terrain-projected data. In the case of ellipsoid-projected data there will be some offsets in the relative band-to-band registration due to the parallax caused by the true height of the viewing surface and physical band separation in the focal plane. Additionally, slight errors in registration can cause a small displacement (on the order of a degree or two) of polarimetric features such as the backscatter glory from their expected location.

Occasional gaps of isolated lines in AirMSPI pushbroom imagery are present. These are due to changes in the ER-2 pitch attitude that occurred too abruptly (e.g., as the result of turbulence) to either: 1) be captured accurately in the ER-2 navigation data, and/or 2) cause gaps in imagery created in a pushbroom fashion.

6 INCIDENTAL DATA QUALITY ISSUES

Occasionally, scene elements (e.g., deep clouds or sunglint) are so bright as to cause saturation in some pixels. Future versions of the AirMSPI product may flag these situations, but this has not been done for the current version of the publicly available data. Isolated pixels that experienced saturation in one or more channels are readily identifiable in the imagery due to their anomalous appearance. Saturated pixels report Not a Number (NaN) values in the HDF files and appear as black pixels in the JPG quicklook images. A list of ACEPOL images containing significant saturation is provided in Appendix B. In other cases, users may notice that the files corresponding to the aftmost angles are shorter than normal, or missing. This can occur, for instance, when the step-and-stare observing sequence was terminated early by the ER-2 pilot.

7 REFERENCES

Diner, D.J., A. Davis, B. Hancock, G. Gutt, R.A. Chipman, and B. Cairns (2007). Dual photoelastic modulator-based polarimetric imaging concept for aerosol remote sensing. *Appl. Opt.* **46**, 8428-8445.

Diner, D.J., A. Davis, B. Hancock, S. Geier, B. Rheingans, V. Jovanovic, M. Bull, D.M. Rider, R.A. Chipman, A. Mahler, and S.C. McClain (2010). First results from a dual photoelastic modulator-based polarimetric camera. *Appl. Opt.* **49**, 2929-2946.

Diner, D.J., F. Xu, J.V. Martonchik, B.E. Rheingans, S. Geier, V.M. Jovanovic, A. Davis, R.A. Chipman, and S.C. and McClain (2012). Exploration of a polarized surface bidirectional reflectance model using the Ground-based Multiangle SpectroPolarimetric Imager. *Atmosphere* **3**, 591-619.

Diner, D.J., F. Xu, M.J. Garay, J.V. Martonchik, B.E. Rheingans, S. Geier, A. Davis, B.R. Hancock, V.M. Jovanovic, M.A. Bull, K. Capraro, R.A. Chipman, and S.C. McClain (2013a). The Airborne Multiangle SpectroPolarimetric Imager (AirMSPI): a new tool for aerosol and cloud remote sensing. *Atmos. Meas. Tech*. **6**, 2007-2025.

Diner, D.J., M.J. Garay, O.V. Kalashnikova, B.E. Rheingans, S. Geier, M.A. Bull, V.M. Jovanovic, F. Xu, C.J. Bruegge, A. Davis, K. Crabtree, and R.A. Chipman (2013b). Airborne Multiangle SpectroPolarmetric Imager (AirMSPI) observations over California during NASA's Polarimeter Definition Experiment (PODEX). *SPIE Proc*. **8873**, 88730B-2.

Jovanovic, V.M., M. Bull, D.J. Diner, S. Geier, and B. Rheingans (2012). Automated data production for a novel Airborne Multiangle SpectroPolarimetric Imager (AirMSPI). *Int. Arch. Photogramm. Remote Sens. Spatial Inf. Sci.*, **XXXIX-B1**, 33-38.

Mahler, A., D.J. Diner, and R.A. Chipman (2011). Analysis of static and time-varying polarization errors in the multiangle spectropolarimetric imager. *Appl. Opt.* **50**, 2080-2087.

Palmer, J.M. (1984). Effective bandwidths for LANDSAT-4 and LANDSAT-D' Multispectral Scanner and Thematic Mapper subsystems. *IEEE Trans. Geosci. Rem. Sens.* **GE-22**, 336-338.

Wehrli, C. (1985). "Extraterrestrial Solar Spectrum", Publication no. 615, Physikalisch Meteorologisches Observatorium + World Radiation Center (PMO/WRC) Davos Dorf, Switzerland, July 1985.

Xu, F., A.B. Davis, R.A. West, and L.W. Esposito (2010). Markov chain formalism for polarized light transfer in plane-parallel atmospheres, with numerical comparison to the Monte Carlo method, *Opt. Express* **19**, 946-967.

8 APPENDIX A: ACRONYM LIST

ACEPOL	Aerosol Characterization from Polarimeter and Lidar
AFRC	Armstrong Flight Research Center
AirMSPI	Airborne Multiangle SpectroPolarimetric Imager
AoLP	Angle of Linear Polarization
ASD	Analytical Spectral Devices
ASDC	Atmospheric Science Data Center
AU	Astronomical Unit
DEM	Digital Elevation Model
DN	Digital Number
DoLP	Degree of Linear Polarization
EOS	Earth Observing System
GCP	Ground Control Point
HDF-EOS	Hierarchical Data Format for EOS
JPL	Jet Propulsion Laboratory
LaRC	Langley Research Center (NASA)
LED	Light Emitting Diode
MISR	Multi-angle Imaging SpectroRadiometer
NaN	Not a Number
NASA	National Aeronautics and Space Administration
NED	National Elevation Dataset
NIST	National Institute of Standards and Technology
PEM	Photoelastic Modulator
RDQI	Radiometric Data Quality Indicator
SCF	Science Computing Facility
SDP	Science Data Processing
SI	*Système international*
SRF	Spectral Response Function
USGS	United States Geological Survey
UTM	Universal Transverse Mercator
UV	Ultraviolet
WGS84	World Geodetic System 1984

9 APPENDIX B

Images containing saturated pixels:

AirMSPI_ER2_GRP_ELLIPSOID_20171019_174039Z_CA-Mojave_SWPA_F01_V006
AirMSPI_ER2_GRP_ELLIPSOID_20171023_212848Z_CA-Avalon_SWPA_F01_V006
AirMSPI_ER2_GRP_ELLIPSOID_20171023_212933Z_CA-Avalon_SWPF_F01_V006
AirMSPI_ER2_GRP_ELLIPSOID_20171023_213527Z_NorthPacificOcean-34N118W_490A_F01_V006
AirMSPI_ER2_GRP_ELLIPSOID_20171023_213556Z_NorthPacificOcean-34N118W_553A_F01_V006
AirMSPI_ER2_GRP_ELLIPSOID_20171023_213626Z_NorthPacificOcean-34N118W_604A_F01_V006
AirMSPI_ER2_GRP_ELLIPSOID_20171023_213659Z_NorthPacificOcean-34N118W_645A_F01_V006
AirMSPI_ER2_GRP_ELLIPSOID_20171023_213740Z_CA-YorbaLinda_SWPF_F01_V006
AirMSPI_ER2_GRP_ELLIPSOID_20171025_180227Z_CA-Rosamond_553A_F01_V006
AirMSPI_ER2_GRP_ELLIPSOID_20171025_195942Z_CA-Bakersfield_458A_F01_V006
AirMSPI_ER2_GRP_ELLIPSOID_20171107_181552Z_CA-SantaAna_SWPF_F01_V006
AirMSPI_ER2_GRP_ELLIPSOID_20171107_183711Z_CA-HuntingtonBeach_490A_F01_V006
AirMSPI_ER2_GRP_ELLIPSOID_20171107_183740Z_CA-HuntingtonBeach_553A_F01_V006
AirMSPI_ER2_GRP_ELLIPSOID_20171107_183810Z_CA-HuntingtonBeach_604A_F01_V006
AirMSPI_ER2_GRP_ELLIPSOID_20171107_183844Z_CA-HuntingtonBeach_645A_F01_V006
AirMSPI_ER2_GRP_ELLIPSOID_20171107_183924Z_CA-LosAngeles_SWPF_F01_V006
AirMSPI_ER2_GRP_ELLIPSOID_20171107_191007Z_CA-Bakersfield_571A_F01_V006
AirMSPI_ER2_GRP_ELLIPSOID_20171107_193417Z_CA-Lemoore_SWPA_F01_V006
AirMSPI_ER2_GRP_ELLIPSOID_20171107_193508Z_CA-Lemoore_SWPF_F01_V006
AirMSPI_ER2_GRP_ELLIPSOID_20171107_194152Z_CA-Fresno_571A_F01_V006
AirMSPI_ER2_GRP_ELLIPSOID_20171107_202932Z_NorthPacificOcean-37N123W_SWPA_F01_V006
AirMSPI_ER2_GRP_ELLIPSOID_20171107_203033Z_NorthPacificOcean-37N123W_SWPF_F01_V006
AirMSPI_ER2_GRP_ELLIPSOID_20171107_203135Z_NorthPacificOcean-38N123W_SWPA_F01_V006
AirMSPI_ER2_GRP_ELLIPSOID_20171107_203236Z_NorthPacificOcean-38N123W_SWPF_F01_V006
AirMSPI_ER2_GRP_ELLIPSOID_20171107_215910Z_CA-Bakersfield_458A_F01_V006